Circadian Gating of the Cell Cycle Revealed in Single Cyanobacterial Cells

Qiong Yang *et al.*

Science **327**, 1522 (2010);
DOI: 10.1126/science.1181759

identified cornichon homologs 2 and 3 (*2*), because CKAMP44 also slows AMPAR deactivation, although in a less pronounced manner, and, similarly to TARPs, CKAMP44 increases glutamate affinity (*3*, *12*, *13*).

However, CKAMP44 differs considerably from other AMPAR auxiliary proteins in its modulation of AMPAR desensitization. It modulates AMPAR function by increasing desensitization, decreasing τ_{des}, and slowing the recovery from desensitization, whereas TARPs and cornichons reduce and slow desensitization (*2*, *3*, *12*). The influence of CKAMP44 on τ_{deact} and τ_{des} is noteworthy, as TARPs and cornichons increase both τ_{deact} and τ_{des} (*2*, *3*, *12*). Coregulation of τ_{deact} and τ_{des} (increase or decrease of both) was also observed for most AMPAR mutations that, for example, influence the dimer interface stability (*14*, *15*). In contrast, AMPAR mutations in the ligand-binding cleft that affect the stability of the closed-cleft conformation (interaction between domains D1 and D2) have opposite effects on τ_{deact} and τ_{des}. Mutations that disrupt interactions between these domains decrease τ_{deact} and increase τ_{des}. In addition, such mutations decrease agonist affinity and also accelerate recovery from desensitization (*16*). Conversely, mutations that stabilize the closed-cleft conformation slow both deactivation and recovery from desensitization, and increase agonist apparent affinity (*17*). Therefore, the effects of CKAMP44 on AMPAR properties are consistent with CKAMP44 stabilizing the closed-cleft conformation of the ligand-binding core.

The role that CKAMP44 exerts on desensitization is opposite to that of TARPs, but cannot be explained by the replacement or elimination of TARPs from the AMPAR complex. According to our coimmunoprecipitation studies, CKAMP44 appears to act on AMPARs associated with TARPs. Moreover, as demonstrated by the comparison of CA1 and DG synapses and the differential expression of CKAMP44, the modulation of AMPARs occurs to different extents at these synapses. By contrast, cornichons and TARPs seem to be essential auxiliary subunits of the AMPAR complex in the central nervous system.

The CKAMP44-mediated increase in AMPAR desensitization influences short-term plasticity of EPSCs by reducing paired-pulse facilitation. In most synapses, short-term plasticity is thought to reflect changes in transmitter release probability. There are only a few synapses for which AMPAR desensitization has been shown to influence PPR (*18*–*20*). Slow recovery from desensitization, pronounced glutamate spillover, and high release probability are thought to enable AMPAR desensitization to influence PPR. As we have demonstrated here, AMPAR desensitization can reduce the PPR in CA1 pyramidal and DG granule cell synapses at physiological temperatures provided that recovery from desensitization is slow. In CA1 neurons, CKAMP44 expression is low and, hence, CKAMP44 overexpression is required to reduce the PPR. In contrast, endogenous CKAMP44 expression in DG granule cells is sufficiently high for CKAMP44 KO to increase PPR. An approximately fourfold slower recovery from desensitization was described for AMPA EPSCs in DG granule cells compared to CA1 pyramidal neurons, which led to the hypothesis that this distinction might underlie the different PPRs in CA1 and DG neurons (*21*). Our data confirm this hypothesis and identify CKAMP44 as the protein that differentially modulates short-term plasticity in these synapses.

References and Notes

1. C. L. Palmer, L. Cotton, J. M. Henley, *Pharmacol. Rev.* **57**, 253 (2005).
2. J. Schwenk *et al.*, *Science* **323**, 1313 (2009).
3. S. Tomita *et al.*, *Nature* **435**, 1052 (2005).
4. S. Tomita *et al.*, *J. Cell Biol.* **161**, 805 (2003).
5. Y. Zheng, J. E. Mellem, P. J. Brockie, D. M. Madsen, A. V. Maricq, *Nature* **427**, 451 (2004).
6. S. H. Heinemann, E. Leipold, *Cell. Mol. Life Sci.* **64**, 1329 (2007).
7. Y. Stern-Bach, S. Russo, M. Neuman, C. Rosenmund, *Neuron* **21**, 907 (1998).
8. N. Pilpel, N. Landeck, M. Klugmann, P. H. Seeburg, M. K. Schwarz, *J. Neurosci. Methods* **182**, 55 (2009).
9. B. L. McNaughton, *Brain Res.* **199**, 1 (1980).
10. C. S. Walker *et al.*, *Curr. Biol.* **19**, 900 (2009).
11. L. Chen, A. El-Husseini, S. Tomita, D. S. Bredt, R. A. Nicoll, *Mol. Pharmacol.* **64**, 703 (2003).
12. A. Priel *et al.*, *J. Neurosci.* **25**, 2682 (2005).
13. M. Morimoto-Tomita *et al.*, *Neuron* **61**, 101 (2009).
14. M. S. Horning, M. L. Mayer, *Neuron* **41**, 379 (2004).
15. K. M. Partin, M. W. Fleck, M. L. Mayer, *J. Neurosci.* **16**, 6634 (1996).
16. A. Robert, N. Armstrong, J. E. Gouaux, J. R. Howe, *J. Neurosci.* **25**, 3752 (2005).
17. M. C. Weston, C. Gertler, M. L. Mayer, C. Rosenmund, *J. Neurosci.* **26**, 7650 (2006).
18. C. Chen, D. M. Blitz, W. G. Regehr, *Neuron* **33**, 779 (2002).
19. L. O. Trussell, S. Zhang, I. M. Raman, *Neuron* **10**, 1185 (1993).
20. M. J. Wall, *Eur. J. Neurosci.* **21**, 2149 (2005).
21. D. Colquhoun, P. Jonas, B. Sakmann, *J. Physiol.* **458**, 261 (1992).

22. We thank M. K. Schwarz for recombinant adeno-associated virus delivery into the brains of mouse pups, A. Zivkovich for electrophysiological experiments during the initial stages of this project, L. Layer and S. Giese for help with molecular cloning, R. van der Schors for his contribution to the mass spectrometry, and R. Hinz-Herkommer, I. Preugschat-Gumprecht, and R. Zilberstein for technical assistance. Supported by the Schilling Foundation (H.M.); EU-Synapse LSHM-CT-2005-019055 (H.M., P.H.S., Y.S.B.); SFB636 (R.S.P.) and Nationales Genomforschungsnetz (NGFN) (R.S.P.); the Center for Medical Systems Biology (K.W.L. and A.B.S.); and the Max Planck Society (R.S.P. and P.H.S.). The experimentally verified cDNA CKAMP44 sequences are annotated at the National Center for Biotechnology Information under the accession numbers GU479981 (CKAMP44a) and GU479982 (CKAMP44b).

Supporting Online Material

www.sciencemag.org/cgi/content/full/science.1184178/DC1
Materials and Methods
SOM Text
Tables S1 to S6
Figs. S1 to S8
References

3 November 2009; accepted 22 January 2010
Published online 25 February 2010;
10.1126/science.1184178
Include this information when citing this paper.

Circadian Gating of the Cell Cycle Revealed in Single Cyanobacterial Cells

Qiong Yang,[1]* Bernardo F. Pando,[1]* Guogang Dong,[2] Susan S. Golden,[2] Alexander van Oudenaarden[1,3]†

Although major progress has been made in uncovering the machinery that underlies individual biological clocks, much less is known about how multiple clocks coordinate their oscillations. We simultaneously tracked cell division events and circadian phases of individual cells of the cyanobacterium *Synechococcus elongatus* and fit the data to a model to determine when cell cycle progression slows as a function of circadian and cell cycle phases. We infer that cell cycle progression in cyanobacteria slows during a specific circadian interval but is uniform across cell cycle phases. Our model is applicable to the quantification of the coupling between biological oscillators in other organisms.

Cyclic processes in biology span a wide dynamic range, from the subsecond periods of neural spike trains to annual rhythms in animal and plant reproduction (*1*–*3*). Even an individual cell exposed to a constant environment may exhibit many parallel periodic activities with different frequencies, such as glycolytic, cell cycle, and circadian oscillations (*4*–*8*). Therefore, it is important to elucidate how different oscillators couple to each other (*9*). In several unicellular organisms and higher vertebrates, it has been shown that the circadian system affects whether cell division is permitted (*10*–*15*); similarly, the yeast metabolic cycle restricts when the cell divides (*16*). Here, we integrate theoretical and experimental approaches to investigate how the circadian and cell division subsystems are coupled together in single cells of the cyanobacterium *Synechococcus elongatus*.

To quantify how one clock couples to the other, we built a model by describing the state of each cell with its circadian phase $\theta(t)$ and cell

[1]Department of Physics, Massachusetts Institute of Technology, Cambridge, MA 02139, USA. [2]Center for Chronobiology and Division of Biological Sciences, University of California, San Diego, La Jolla, CA 92093, USA. [3]Department of Biology, Massachusetts Institute of Technology, Cambridge, MA 02139, USA.

*These authors contributed equally to this work.
†To whom correspondence should be addressed. E-mail: avano@mit.edu

cycle phase $\phi(t)$ both periodic from 0 to 2π (*17*, *18*). Given the robustness of circadian oscillations to environmental and intracellular variations, it is believed that the circadian system progresses independently of the cell cycle (*19*, *20*). Hence, we propose that the progression rate of the circadian phase is constant except for some noise, whereas the speed of cell cycle progression could depend on both the circadian and cell cycle phases. We describe the time evolution of the phases of these clocks by two Langevin equations,

$$\begin{cases} \dfrac{d\theta}{dt} = \nu_0 + \xi_\theta \\ \dfrac{d\phi}{dt} = \nu\gamma(\phi, \theta) + \xi_\phi \end{cases} \quad (1)$$

where ξ_θ and ξ_ϕ are white-noise terms representative of intrinsic fluctuations, ν_0 is the speed of the circadian clock, ν roughly describes the average speed of cell cycle progression, and $\gamma(\phi, \theta)$, the coupling, is a non-negative function describing how the state of the clocks affects cell cycle speed. Regions in (ϕ, θ) space where γ is close to zero indicate slowing of cell cycle progression and are usually referred to as "gates" (*11*).

This model can be simulated using Monte Carlo methods or solved using Fokker-Planck techniques (*21*) to explore whether the cell cycle becomes synchronized to circadian signals and how the timing of cell divisions is distributed throughout the day. A division event happens as the variable ϕ crosses the 2π boundary (*22*). Without gating ($\gamma = 1$), the two clocks are uncorrelated and cells divide uniformly throughout the day (Fig. 1, left column). However, in the presence of a gate, cell cycle states synchronize to the circadian signal (Fig. 1, center column), similarly to how nonlinear oscillators lock into periodic forcings (*23*, *24*). For cell cycle speeds comparable to that of the circadian clock, cells tend to divide at a single circadian phase; however, as ν is increased, the number of times during the day at which divisions are likely to take place also increases, leading to multimodal distributions of division phases (Fig. 1, right column, and fig. S2) (*25*). This feature is generic and independent of the specific shape of the coupling function used (*17*, *18*, *23*) (fig. S8).

To quantify this gating phenomenon experimentally, we investigated the interaction between the circadian and cell cycle clocks in the cyanobacterium *S. elongatus* PCC 7942. A previous study at the population level indicated the existence of circadian gating in this organism (*11*). To explicitly explore how one clock gates the other, we took a single-cell fluorescence microscopy approach and simultaneously tracked both clocks' dynamics in individual cyanobacteria as they proliferated under a constant-light environment (Fig. 2A). Circadian dynamics in each cell are faithfully reported by the SsrA-tagged yellow fluorescent protein (YFP-SsrA) under the rhythmic *kaiBC* promoter (*26*). This promoter drives the endogenous expression of the *kaiB* and *kaiC* genes, which, together with *kaiA*, form the central protein circuit that orchestrates circadian rhythms in cyanobacteria. We defined the circadian phase as the time from the nearest previous YFP peak normalized by the circadian period (Fig. 2B); our proxy for cell cycle phase progression involved tracking individual cells' growth over time (*21*). We detected nearly all cell divisions, recorded the corresponding circadian phases

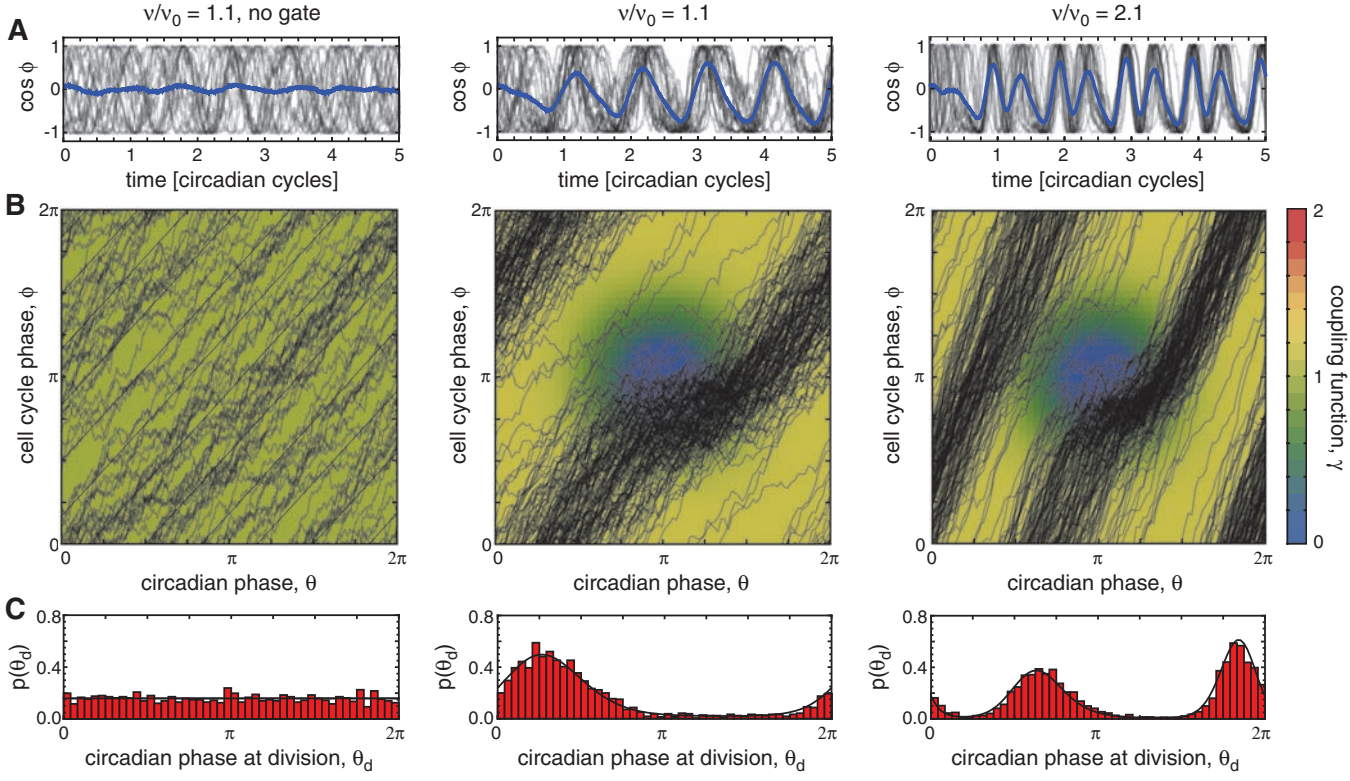

Fig. 1. Synchronization of cell cycle phases to circadian signals. Monte Carlo simulations of the evolution of a population of cells are shown with an initially uniform distribution of cell cycle phases and synchronous circadian signals. (**A**) Cosine projection of cell cycle phases of 10 traces and average across 100 traces. The ratio of the average speed of cell cycle progression and circadian speed ν/ν_0 is 1.1 for the left and center columns and 2.1 for the right column. The left column represents a situation in which there is no gating ($\gamma = 1$); in the other columns, the shape of the coupling function is color-coded in (B). (**B**) Color-coded coupling function and steady-state organization of trajectories in (ϕ, θ) space. In the no-gate case, straight lines show the deterministic behavior. (**C**) Steady-state probability distribution of circadian phases at which divisions take place, $p(\theta_d)$. The bars are the results of Monte Carlo simulations; the solid line represents the result of a Fokker-Planck computation (*21*). Parameters used: $D_\theta = 0$, $D_\phi = 0.1\nu_0$, and, for the center and right columns, $\alpha = \beta = 4$, $\theta_0 = \phi_0 = \pi$, where D_θ and D_ϕ correspond to the noise strengths of the circadian and cell cycle oscillators, and α, β, θ_0, and ϕ_0 are parameters defining the shape and position of the coupling function (*21*).

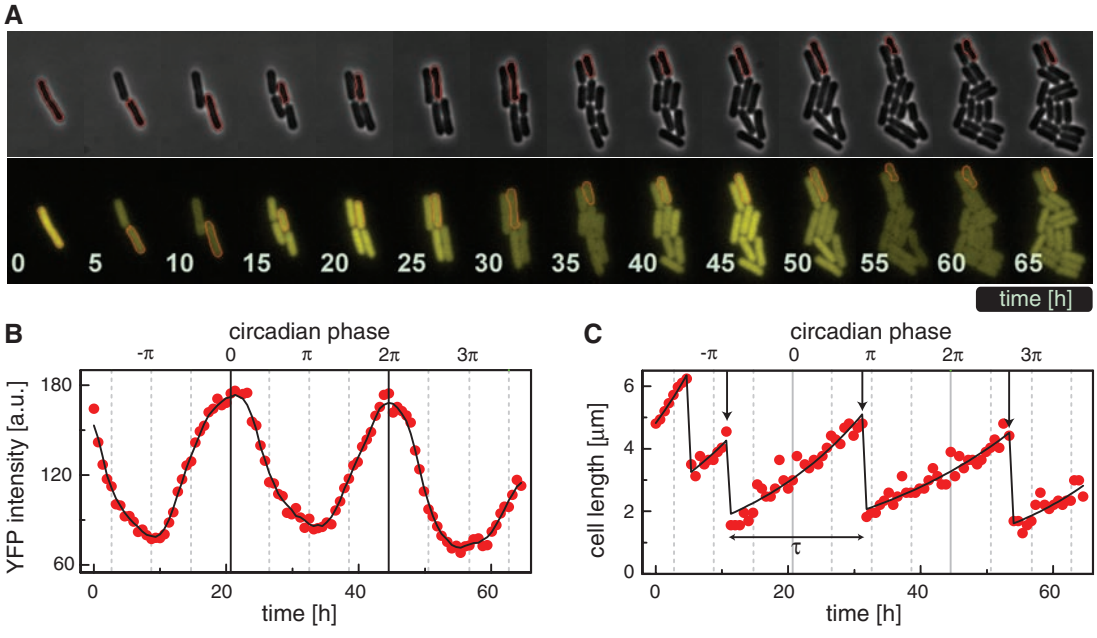

Fig. 2. Time-lapse microscopy allows single-cell measurements of circadian and cell cycle states. (**A**) Phase contrast (upper panel) and YFP images (lower panel) of a colony tracked over a few days. (**B**) YFP trace for the cell outlined in red in (A) (red dots, YFP intensity; black line, 10-point running average). (**C**) Length dynamics of the same cell (dots, instantaneous cell length; black line, exponential fit; vertical arrows, circadian phases at cell divisions; horizontal double arrow, cell cycle duration τ for one cell).

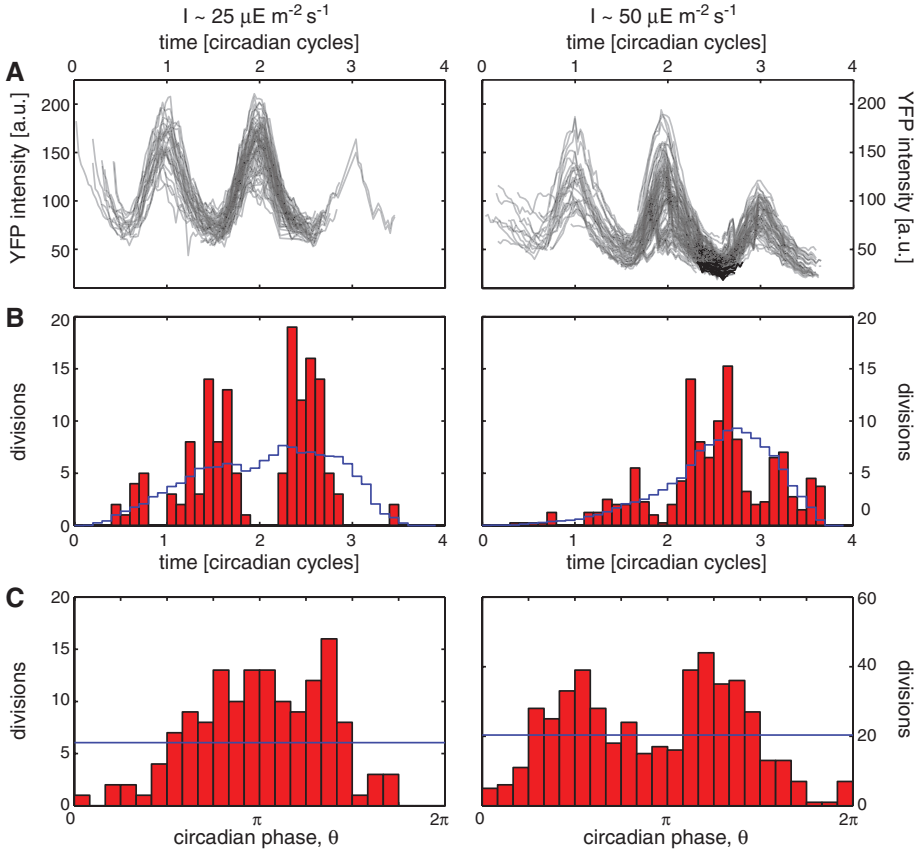

Fig. 3. Circadian gating as observed in single cells. (**A**) YFP traces for cells in 18 colonies shifted so as to maximize overlap. (**B**) Histogram of the timing of division events. Blue trace represents expectation for uncorrelated clocks. (**C**) Histogram of the timing of division events across the circadian cycle; plot constructed as in (B) but measuring time relative to the start of each circadian cycle. Left column: experiment performed under light intensity I ~ 25 μE m^{-2} s^{-1}; right column: I ~ 50 μE m^{-2} s^{-1}.

θ_d, and measured the cell cycle duration τ for each cell (Fig. 2C).

We first performed an experiment under a light intensity of ~25 μE m^{-2} s^{-1} (*27*) (Fig. 3, left column), which gave an average cell cycle speed comparable to that of the circadian clock: τ = 18 ± 7 hours (mean ± SD). To test whether cell cycle phases were indeed synchronized by circadian signals, we collected all single-cell traces, aligned them on the basis of their circadian phases (*21*), and constructed histograms of the circadian phases at division (Fig. 3). Rather than the distribution expected for uncorrelated clocks (*21*), we found a single-peaked distribution of divisions per circadian cycle, indicating that divisions happened mostly at a specific circadian time.

In theory, we expect a similar locking if we double the speed of the cell cycle relative to that of the circadian clock, with divisions taking place at two specific circadian phases. Although the period of the circadian clock is nearly constant over a range of growth conditions, cell cycle progression is sensitive to environmental light intensity. These properties allowed us to tune the

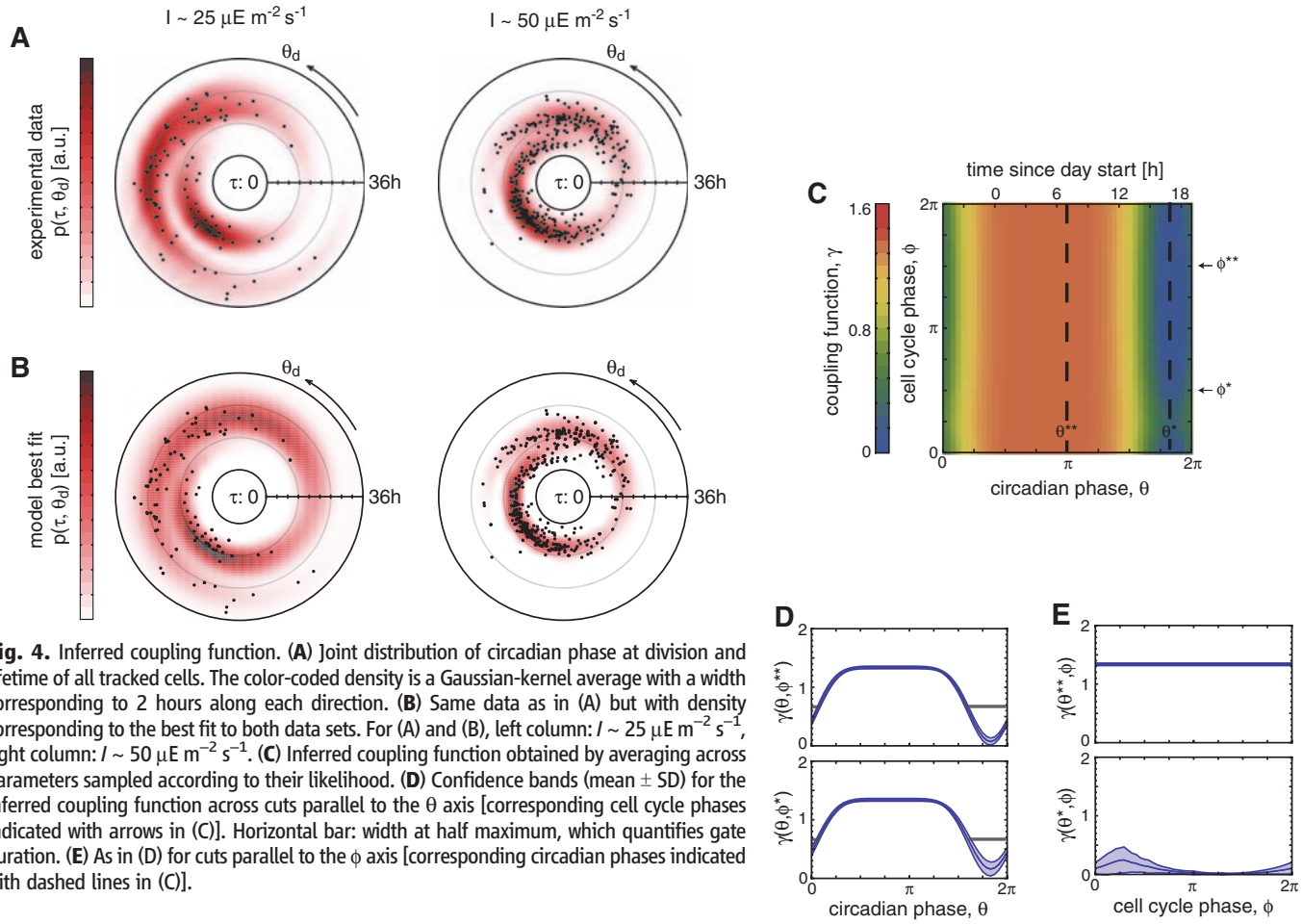

Fig. 4. Inferred coupling function. (**A**) Joint distribution of circadian phase at division and lifetime of all tracked cells. The color-coded density is a Gaussian-kernel average with a width corresponding to 2 hours along each direction. (**B**) Same data as in (A) but with density corresponding to the best fit to both data sets. For (A) and (B), left column: $I \sim 25\ \mu E\ m^{-2}\ s^{-1}$, right column: $I \sim 50\ \mu E\ m^{-2}\ s^{-1}$. (**C**) Inferred coupling function obtained by averaging across parameters sampled according to their likelihood. (**D**) Confidence bands (mean ± SD) for the inferred coupling function across cuts parallel to the θ axis [corresponding cell cycle phases indicated with arrows in (C)]. Horizontal bar: width at half maximum, which quantifies gate duration. (**E**) As in (D) for cuts parallel to the ϕ axis [corresponding circadian phases indicated with dashed lines in (C)].

cell cycle speed while keeping a constant circadian rate. With a light intensity of ~50 $\mu E\ m^{-2}\ s^{-1}$, the average cell cycle duration shortened to 10 ± 4 hours (mean ± SD), whereas the average circadian period stayed around 24 hours. Hence, we obtained a factor of ~2 increase in the relative speed of the two oscillators. We observed two peaks of cell divisions per circadian cycle (Fig. 3), in agreement with our theoretical analysis (Fig. 1).

A better understanding of the gating phenomenon relies on a direct measurement of the correlation between the two clocks for each single cell. We summarized such interaction in scatterplots of the circadian phase at cell division, θ_d, and the cell cycle duration of the corresponding cell, τ (Fig. 4A). We fit our model to both data sets simultaneously, considering the same coupling function $\gamma(\phi, \theta)$ and noise strengths for the two experiments. We allowed only the parameter ν to vary across the two experimental conditions and included only coupling functions representative of a single maximal gate (*21*). This procedure yielded reasonable fits for both data sets (Fig. 4B), indicating that it is possible to explain the interaction between the clocks in the two different conditions using the same coupling function.

The inferred coupling function is shown in Fig. 4C. To relate the phase θ to the real circadian phase, we considered that the YFP protein has a non-negligible lifetime, which makes the reported signal lag behind the day-night cycle. Measurements on cell cultures that had been synchronized by three 12:12 light-dark cycles indicate that the signal peak (identified as θ = 0) lags (19 ± 1 hours) behind the day start (*21*), in agreement with previous studies (*26*). Considering this delay, the inferred coupling function shows a gate positioned at 17 hours after the day start, lasting for 6.1 ± 0.3 hours (Fig. 4D) and distributed essentially uniformly across cell cycle stages (Fig. 4E). We conclude that in this case the circadian signal acts on the cell cycle by repressing essentially all its stages in the middle of the subjective night.

This suggests that in *Synechococcus*, regulation of cell cycle progression by the circadian system may be more extensive than interactions between circadian signals and proteins associated with specific cell cycle processes. The molecular mechanism coupling the two oscillators in *Synechococcus* might be fundamentally different from that found in mammalian cells in which the expression of several key cell cycle regulators, including Wee1 and Cdc2, was found to be regulated by the circadian oscillator (*12*). Recent data have begun to reveal molecular interactions responsible for coupling the cell cycle and the circadian oscillator in cyanobacteria (*28*). Our results suggest that it is unlikely that gating is exclusively regulated by just one mechanism that imposes a checkpoint at a specific cell cycle stage. Instead, a more overarching regulation scheme may be involved, perhaps analogous to how circadian clocks coordinate genome-wide gene expression at specific circadian times (*29*).

The gating phenomenon seems to be universally conserved from some prokaryotes to mammals. It would be interesting to understand why gating is important to cells. In cyanobacteria, cells enhance their fitness when their circadian period resonates with external light-dark cycles (*30*), and perhaps a similar resonance between circadian and cell cycle clocks might lead to a fitness increase. Consistent with this finding, our results suggest that cell growth is prohibited during the middle of the night when energy is most limited.

The proposed theoretical approach is generally applicable to any set of coupled cyclic processes in which some information about the phases of each clock could be independently

measured. We expect that its use will lead to a deeper understanding of how multiple periodic processes coordinate to control the dynamic state of the cell.

References and Notes

1. A. Goldbeter, *Biochemical Oscillations and Cellular Rhythms: The Molecular Bases of Periodic and Chaotic Behaviour* (Cambridge Univ. Press, Cambridge, 1996).
2. L. Glass, M. C. Mackey, *From Clocks to Chaos: The Rhythms of Life* (Princeton Univ. Press, Princeton, NJ, 1988).
3. M. Maroto, N. A. M. Monk, *Cellular Oscillatory Mechanisms* (Springer Science+Business Media, New York, 2008).
4. O. Dyachok, Y. Isakov, J. Sågetorp, A. Tengholm, *Nature* **439**, 349 (2006).
5. B. N. Kholodenko, *Nat. Rev. Mol. Cell Biol.* **7**, 165 (2006).
6. S. Panda, J. B. Hogenesch, S. A. Kay, *Nature* **417**, 329 (2002).
7. A. Goldbeter, *Curr. Biol.* **18**, R751 (2008).
8. M. Ishiura *et al.*, *Science* **281**, 1519 (1998).
9. S. Méndez-Ferrer, D. Lucas, M. Battista, P. S. Frenette, *Nature* **452**, 442 (2008).
10. E. Nagoshi *et al.*, *Cell* **119**, 693 (2004).
11. T. Mori, B. Binder, C. H. Johnson, *Proc. Natl. Acad. Sci. U.S.A.* **93**, 10183 (1996).
12. T. Matsuo *et al.*, *Science* **302**, 255 (2003).
13. M. P. S. Dekens *et al.*, *Curr. Biol.* **13**, 2051 (2003).
14. J. Hirayama, L. Cardone, M. Doi, P. Sassone-Corsi, *Proc. Natl. Acad. Sci. U.S.A.* **102**, 10194 (2005).
15. M. G. Salter, K. A. Franklin, G. C. Whitelam, *Nature* **426**, 680 (2003).
16. B. P. Tu, A. Kudlicki, M. Rowicka, S. L. McKnight, *Science* **310**, 1152 (2005).
17. A. T. Winfree, *The Geometry of Biological Time* (Springer-Verlag, Rensselaer, NY, 1980).
18. H. S. Strogatz, *Nonlinear Dynamics and Chaos* (Perseus, Cambridge, MA, 1994).
19. T. Mori, C. H. Johnson, *J. Bacteriol.* **183**, 2439 (2001).
20. I. Mihalcescu, W. Hsing, S. Leibler, *Nature* **430**, 81 (2004).
21. See supporting material on *Science* Online.
22. The validity of this identification is independent of the relationship between phases inside this range and specific biological processes.
23. L. Glass, *Nature* **410**, 277 (2001).
24. G. Charvin, F. R. Cross, E. D. Siggia, *Proc. Natl. Acad. Sci. U.S.A.* **106**, 6632 (2009).
25. J. Zámborszky, C. I. Hong, A. Csikász Nagy, *J. Biol. Rhythms* **22**, 542 (2007).
26. J. R. Chabot, J. M. Pedraza, P. Luitel, A. van Oudenaarden, *Nature* **450**, 1249 (2007).
27. $\mu E\ m^{-2}\ s^{-1}$ is a measure of light intensity, where E represents an Einstein unit (one mole of photons).
28. G. Dong *et al.*, *Cell* **140**, 529 (2010).
29. K. Imai, T. Nishiwaki, T. Kondo, H. Iwasaki, *J. Biol. Chem.* **279**, 36534 (2004).
30. Y. Ouyang, C. R. Andersson, T. Kondo, S. S. Golden, C. H. Johnson, *Proc. Natl. Acad. Sci. U.S.A.* **95**, 8660 (1998).

31. We thank J. Gore, P. Luitel, C. Engert, and S. Klemm for helpful discussions and/or experimental help. Supported by NSF grant PHY-0548484 and by NIH grants R01-GM068957 and R01-GM062419.

Supporting Online Material

www.sciencemag.org/cgi/content/full/327/5972/1522/DC1
Materials and Methods
Figs. S1 to S11
Tables S1 to S4
References

10 September 2009; accepted 16 February 2010
10.1126/science.1181759